Computational Strategies Improvement for the Generalized PEEC Method

Jean Michel Guichon, Kouceila Alkama, Gérard Meunier, Olivier Chadebec, Jean-Michel Guichon, Bertrand Bannwarth, Enrico Vialardi, Remy Perrin-Bit

COMPUTATIONAL STRATEGIES IMPROVEMENT FOR THE UNSTRUCTURED INDUCTIVE PEEC METHOD

Kouceila Alkama[1,2], Gérard Meunier[1], Olivier Chadebec[1], Jean-Michel Guichon[1], Bertrand Bannwarth[1], Enrico Vialardi[2], Rémy Perrin-Bit[2]
[1]Univ. Grenoble Alpes, CNRS, Grenoble INP, G2Elab, 38000 Grenoble, France
[2]Altair Engineering France, 38240 Meylan, France

Computational strategies improvements for the inductive unstructured PEEC method are presented in order to address efficiently low frequencies electromagnetic problems. Couplings between volume, surface and line regions have been developed to reduce the number of degrees of freedom and thus the computational cost. Good accuracy on results is ensured thanks to the use of an adaptive Gauss integration procedure for the computation of near interactions. Multi-threaded AMLFMM matrix compression algorithm is used to speed-up far interactions computation. External circuit components can also be coupled to the meshed conductive regions.

***Index Terms*—Quasi-static, Integral Method, Unstructured Partial Element Equivalent Circuit (PEEC) method, AMLFMM.**

I. INTRODUCTION

THE Partial Element Equivalent Circuit (PEEC) method has been shown to be well suited for the analysis of many Electromagnetic (EM) devices, such as busbars, PCBs, integrated circuit interconnects, packaging and others [1]. These devices have a rather plane geometry and their conductive parts are separated by a large amount of surrounding air, which is not necessary to mesh when using PEEC method, being an integral technique. This characteristic represents one of the main advantages of PEEC, along with its ability to couple with electric circuits, thanks to the fact that PEEC formulation transforms Maxwell's equations on the active domain into an equivalent circuit representation. The standard PEEC method has been first introduced by A. E. Ruehli [2]. The principle is to discretize the geometries with a Manhattan-type mesh. Piecewise constant basis functions are used to expand the current density in elements. It limits the method to simple geometries, by forcing the user to make many simplifications if complex devices are under consideration even if a non-orthogonal PEEC formulation has been developed in [3] allowing to gain a little more flexibility. Furthermore, an unstructured PEEC method has been developed [4], [5], removing the limitation of simple geometries, thus allowing the use of PEEC for the modeling a wider range of EM applications. Unstructured PEEC is based on 2-form Whitney face shape functions [6] in order to interpolate the current density $\mathbf{J}$. This approach provides a solution that ensures by construction the conservation of the current through the faces of the unstructured mesh, as in [7], [8] for conductive medias. Later, extensions to dielectric [5], [9] and magnetic materials [10] have been proposed. Thin electromagnetic media modeling has been introduced in [11], and also Surface Impedance Boundary Condition formulations (SIBC) in [12]. All these improvements lead to a general and robust formulation allowing to consider PEEC method as a direct concurrent to the Finite Element Method (FEM).

However, the use of integral methods still presents a major drawback: dense matrices are generated during the resolution, leading to a parabolic increase of memory resources and of the computing time. In fact, the PEEC method requires the computation of the interactions between all elements of the mesh, unlike the FEM which only needs the computation of close neighboring interactions leading to sparse matrices. Fortunately, this major drawback has been overcome thanks to efficient matrix compression algorithms.

In this paper, only quasi-static unstructured PEEC inductive formulation is used. The capacitive effects and the propagation phenomena are neglected since this assumption is known to be efficient to model many low-frequency EM devices. From a computational point of view, it has to keep in mind that integral methods are more complex to implement compared to FEM, the main difficult being the computation of the Green's kernel which may lead to singular integrals. This implies that only few commercial tools based on such integral techniques are usable in a complex industrial environment, because ensuring in any cases their robust implementation as well as a very good accuracy remains a challenging task.

Computational strategies improvements in terms of accuracy and computation speed have to be developed and some original contributions are proposed in this paper, where couplings between volume, surface (shell and SIBC) and line regions are considered in order to reduce the number of degrees of freedoms (DOFs), to accurately integrate the interactions between these regions, an adaptive Gauss points integration procedure has been developed to ensure it. In addition to this accuracy considerations, in order to keep the computation time and the memory consumption as low as possible, an Adaptive Multi Level Fast Multipole Method (AMLFMM) [13] is used as compression algorithm, combined with a multi-threaded CPU parallelization strategy, with an iterative solver FGMRES to solve the linear system obtained and with an efficient preconditionning technique for fastest convergences. All these combined strategies enable a performant simulation of complex power electronics devices with a large number of DOFs. This paper is structured as follows. In Section II, the quasi-static (or inductive) unstructured PEEC formulation is presented. Section III presents the different computational im-

provement strategies. Section IV shows numerical examples. Finally a conclusion is given in Section V.

II. Quasi-static unstructured inductive PEEC fomulation

Considering Maxwell's equations under quasi-static assumption, in a conductive domain $\mathbf{\Omega}$, the electric field $\mathbf{E}$ is:

$$\mathbf{E}_{(P)} = -j\omega\mathbf{A}_{(P)} - \nabla \mathrm{V}_{(P)} \tag{1}$$

where $\mathbf{A}$ is the magnetic vector potential, V is the electric scalar potential, and ω is the angular frequency. Considering $\mathbf{J}$ the current density, the magnetic vector potential $\mathbf{A}$ is

$$\mathbf{A}_{(P)} = \frac{\mu_0}{4\pi}\int_{\Omega}\frac{\mathbf{J}_{(Q)}}{r}d\Omega \tag{2}$$

where r is the distance between integration Q and observation P points. Considering the following linear constitutive law

$$\mathbf{J} = \sigma \cdot \mathbf{E} \tag{3}$$

for $\mathbf{\Omega}$, and introducing equations (2) and (3) in (1), we get

$$\frac{\mathbf{J}_{(P)}}{\sigma_{(P)}} = -j\omega\frac{\mu_0}{4\pi}\int_{\Omega}\frac{\mathbf{J}_{(Q)}}{r}d\Omega - \nabla V_{(P)} \tag{4}$$

As proposed in [8], the current density $\mathbf{J}$ is interpolated with first-order face shape functions such as

$$\mathbf{J} = \sum_i \mathbf{w}_i I_i \tag{5}$$

where $\mathbf{w}_i$ is the face shape function and I_i the current flowing through the face i. Applying a standard Galerkin projection procedure to (4) and using $\mathbf{w}$ as projection functions, a matrix system is obtained.

$$\left([\mathbf{R}] + j\omega\,[\mathbf{L}]\right)\{I\} = \{\delta \mathrm{U}\} \tag{6}$$

$$\begin{cases} [\mathbf{R}]_{i,j} = \int_{\Omega}\frac{\mathbf{w}_i\mathbf{w}_j}{\sigma}d\Omega \\ [\mathbf{L}]_{i,j} = \frac{\mu_0}{4\pi}\int_{\Omega}\mathbf{w}_i\int_{\Omega}\frac{\mathbf{w}_j}{r}d\Omega d\Omega \\ \{\delta \mathrm{U}\}_i = -\int_{\Omega}\mathbf{w}_i\nabla V d\Omega \end{cases} \tag{7}$$

For boundary faces of $\mathbf{\Omega}$ not connected to the external circuit, the flowing current has to be imposed to zero using (8), where $\mathbf{n}$ is the external normal.

$$\mathbf{J}\cdot\mathbf{n} = 0 \tag{8}$$

Matrix system (6) can be seen as a classical circuit matrix system $\mathbf{ZI} = \mathbf{U}$, where each unstructured mesh element is associated to its equivalent circuit representation, as shown in Fig.1. This equivalent circuit is composed of one resistance

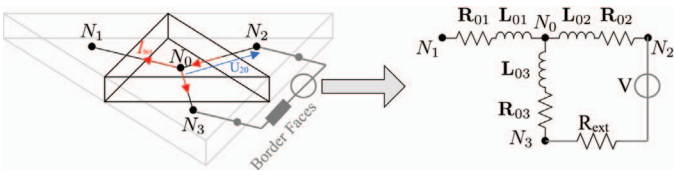

Fig. 1. Equivalent circuit representation for an unstructured mesh

and one self inductance for each face of the mesh element and is completed by all mutual inductances. The outgoing branches of the domain borders allow an easy coupling with external circuit components (source, resistance, inductance and capacitance) as shown in Fig. 1. The circuit is solved with mesh current analysis so in a new base of independent loop currents. To determine the loop, a loop search algorithm is used making possible to deal with multiply connected conductive regions.

III. Integration strategies for PEEC

In this section, an heterogeneous mesh with different types of elements and region dimensions is considered. The integration of the singular Green's kernel presents a major challenge in presence of disparate element presenting large differences in terms of size. The formulation must manage the elements heterogeneity by providing a robust integration of interaction in any cases. In the matrix system (6), the sparse matrix $\mathbf{R}$ is obtained by a finite element integration, but it presents some specifics for elements associated to line, thin and SIBC regions. Another difficulty lies in computing the full matrix $\mathbf{L}$. Strategies for improving these computations are proposed.

A. Integration of $\mathbf{R}$ matrix

Table I presents the $\mathbf{R}$ expressions for volume, surface and line type. For volume element a standard FEM integration process is used. An equivalent conductivity σ^* is introduced to manage skin effects in the case of shell regions [11], and to manage SIBC problems [12]. $\mathbf{e}$ and $\mathbf{s}$ are the thickness and the cross-section for surface and line regions respectively.

TABLE I
Volume, surface and line region type resistive matrices

Types	$\mathbf{J}$ Interpolation	$\mathbf{w_i}$ unit	$R_{i,j}$ term
Volume	$\sum_i \mathbf{w}_{iv} I_i$	$\mathbf{m^{-2}}$	$\int_{\Omega^v}\frac{\mathbf{w}_i\mathbf{w}_j}{\sigma}d\Omega$
Surface	$\frac{1}{e}\sum_i \mathbf{w}_{is} I_i$	$\mathbf{m^{-1}}$	$\int_{\Omega^s}\frac{\mathbf{w}_i\mathbf{w}_j}{e\sigma^*}d\Omega$
Line	$\frac{1}{s}\sum_i \mathbf{w}_{il} I_i$	-	$\int_{\Omega^l}\frac{\mathbf{w}_i\mathbf{w}_j}{s\sigma}d\Omega$

B. Adaptive Gauss points procedure for $\mathbf{L}$ matrix

Improving the computation of partial inductances is more delicate. Analytical correction [14] on source elements and numerical integration for target elements are used in order to increase the precision and reduce the risks of singularity. For the numerical integration, Gaussian-Legendre quadrature methods are used. For each type of mesh element, an associated Gauss point table is defined. The convergence test of a source-target interaction (eS,eT) is made considering the elementary inductance matrix and calculating the relative error ϵ between the current iteration i and the previous iteration i-1.

$$\epsilon = \frac{||\mathbf{L}_{i-1}^{eS,eT} - \mathbf{L}_{i}^{eS,eT}||}{||\mathbf{L}_{i}^{eS,eT}||} \tag{9}$$

As indicated in the diagram of Fig. 2, in order to speed-up the procedure, at each start of a new iteration, the source element loop is updated with the source elements for which the source-target interactions have not yet converged in the previous iteration and the number of Gauss points is increased until the total convergence is reached. Thus, the number of

iterations required is different and adapted to each interaction (e,g two close elements require more iterations than two distant elements) A special care is paid for line mesh elements: a volume representation is automatically generated from their section and $\mathbf{J}$ is assumed to be uniform in the volume. The adaptive integration is then used enabling an accurate computation of the self-inductance which would be singular if a wire without section was considered.

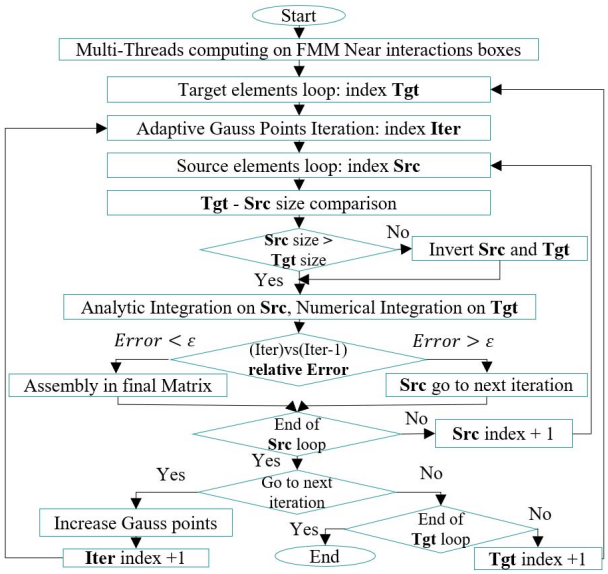

Fig. 2. Diagram of the adaptive Gauss points procedure with FMM

C. Semi-analytical integration sequence optimisation

The sequence of semi-analytical integration between two elements of any type is optimized by inverting source and target element in order to provide a more performing computation. The analytical integration (source) is applied to the largest element to avoid the generation of a high number of Gauss points. The radii of the spheres surrounding the elements are calculated, the element is considered large if its radius is equal to or greater than twice the other. For the sake of simplicity, the line conductors in Fig. 3 are taken as an example. The red line conductor is much longer than the black one and both are located close each other. The spatial distribution of the magnetic vector potential on their median axes is plotted and the convergence of self and mutual inductance computation according to Gauss points number is studied.

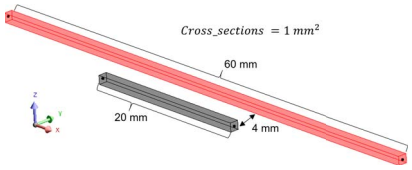

Fig. 3. Two parallel line conductors

1) Mutual inductance computation behaviour

As shown in Fig.4, the magnetic vector potential varies a lot when the black conductor is the source element, implying a large Gauss points number to accurately integrate it as shown in Fig. 5. On the contrary, if the red conductor is the source one, the potential varies little, implying few Gauss points.

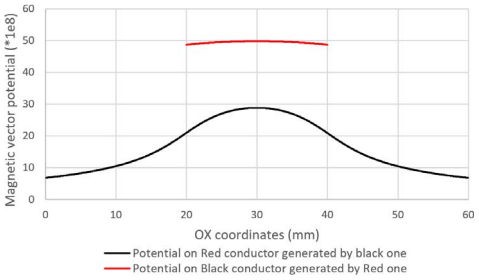

Fig. 4. Magnetic vector potentials on the two line conductors

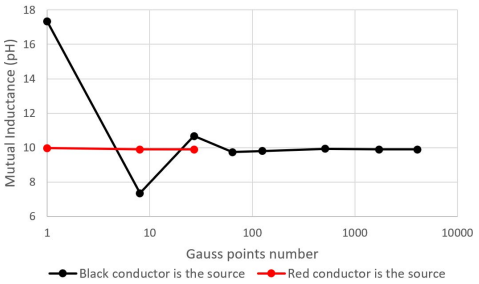

Fig. 5. Mutual inductance between the line conductors ($\epsilon = 1e-3$)

2) Self-inductance computation behaviour

As presented in Fig. 6, the adaptive strategy for the number of Gauss points is very important to correctly calculate the partial self-inductance of a mesh element especially when this element is rather large. Important errors can be obtained if adaptive integration technique is not used (more than 10 percents in the presented case). It demonstrates the interest of our technique which is generalised to all element types.

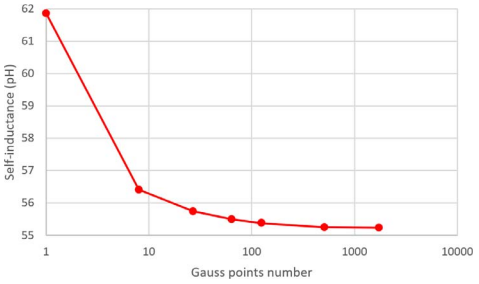

Fig. 6. Self-inductance for the red line conductor ($\epsilon = 1e-3$)

D. Global resolution strategy

The matrix system (7) is solved with FGMRES iterative solver. It guarantees a safe convergence, but can be very slow if the number of unknowns is large and if it is ill-preconditioned. Memory space and computing time are reduced thanks to AMLFMM compression algorithm, far interactions being approximated using a set of spherical expansion. According to our experience, AMLFMM is very competitive in comparison with H-matrix in terms of integration time and memory consumption. For the near interactions, the above integration strategies have been used to preserve a good accuracy of computation, as in Fig. 2. A preconditioning matrix is built from the sum of the sparse matrix $\mathbf{R}$ and the near-inductance terms of $\mathbf{L}$. LU-MUMPS decomposition have been used of this matrix as preconditioning, leading to a consequent reduction

of the solver iterations number. The integration of these techniques inside the software Altair **Flux**™ [15] is envisioned.

IV. Numerical Examples

A. Simple test case

A simple example is presented in Fig. 7. It shows the inductive coupling between a conductive line and a thin region with elements of different sizes. The line coil is supplied by an 1V voltage source at 1000 Hz. Fig. 8 presents the results

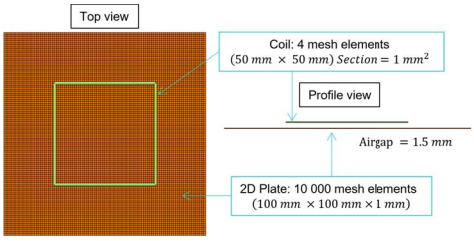

Fig. 7. Simple test case (Thin 2D plate and line Coil)

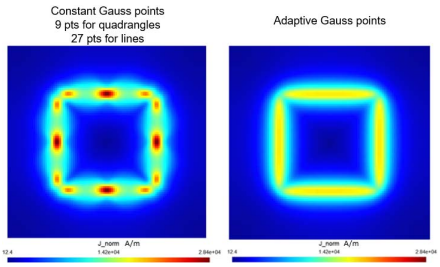

Fig. 8. Eddy current distribution for the standard and the adaptive methods

obtained without and with adaptive methods. The computation time was not strongly affected, **66** seconds for the conventional integration and **83** seconds for the adaptive methods, but the accuracy on eddy current results is greatly increased (see right picture of Fig. 8).

B. Laminated Busbars

In Fig. 9, a problem with an industrial complexity has been solved. It has been meshed with approximately 129,000 elements. It includes several connections with circuit type components (resistances, capacitances). IGBT and diodes have been modeled by their ON-state internal resistances. A laptop with an Intel® Core™ i7-7820HQ CPU @2.90GHz processor with 64 GB of RAM has been used to solve the problem in 20 minutes.

V. Conclusion

Improvement strategies for the unstructured PEEC method have been presented. Couplings between volume, surface and line regions have been proposed in order to reduce DOFs number. An adaptive Gauss points procedure has been developed. It increases the computation precision, and especially allows to correct possible singularities when the size of the mesh elements differs greatly. Multi-threaded AMLFMM algorithm has been used to reduce computation time and memory resources. Finally, two test cases have been treated effectively, demonstrating the power of the unstructured PEEC formulation and the proposed methods.

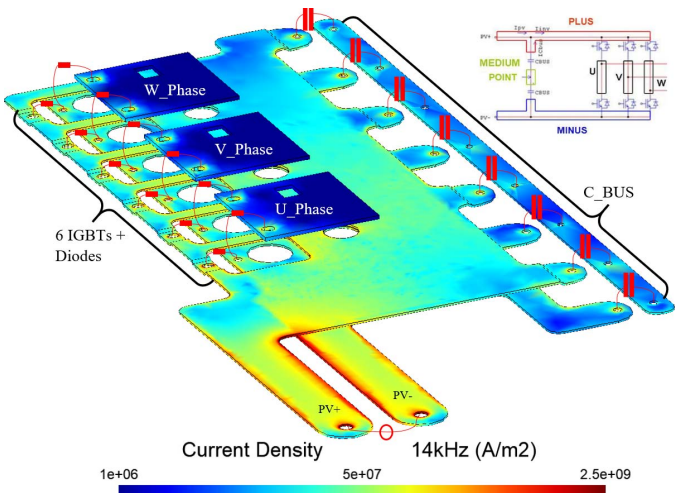

Fig. 9. Distribution of the current density on the laminated busbars when supplied by a voltage source of 100 V at 14 kHz

References

[1] W. F. Bikinga, K. Alkama, B. Mezrag, J. M. Guichon, and Y. Avenas, "Implementation of TAPIR Switching Cells with Integrated Direct Air-Cooling for SiC Power Devices," in *2020 22nd Eur. Conf. Power Electron. Appl. (EPE'20 ECCE Eur.* IEEE, sep 2020, pp. P.1–P.9.

[2] A. E. Ruehli, "Inductance Calculations in a Complex Integrated Circuit Environment," *IBM J. Res. Dev.*, vol. 16, no. 5, pp. 470–481, sep 1972.

[3] A. E. Ruehli, G. Antonini, J. Esch, J. Ekman, A. Mayo, and A. Orlandi, "Nonorthogonal PEEC formulation for time- and frequency-domain EM and circuit modeling," *IEEE Trans. Electromagn. Compat.*, vol. 45, no. 2, pp. 167–176, 2003.

[4] F. Freschi, G. Gruosso, and M. Repetto, "Unstructured PEEC formulation by dual discretization," *IEEE Microw. Wirel. Components Lett.*, vol. 16, no. 10, pp. 531–533, 2006.

[5] J. Siau, G. Meunier, O. Chadebec, J.-M. Guichon, and R. Perrin-Bit, "Volume Integral Formulation Using Face Elements for Electromagnetic Problem Considering Conductors and Dielectrics," *IEEE Trans. Electromagn. Compat.*, vol. 58, no. 5, pp. 1587–1594, oct 2016.

[6] A. Demenko and J. K. Sykulski, "Geometric formulation of edge and nodal finite element equations in electromagnetics," *COMPEL - Int. J. Comput. Math. Electr. Electron. Eng.*, vol. 31, no. 5, sep 2012.

[7] P. Alotto, D. Desideri, F. Freschi, A. Maschio, and M. Repetto, "Dual-PEEC modeling of a two-port TEM cell for VHF applications," *IEEE Trans. Magn.*, vol. 47, no. 5, pp. 1486–1489, 2011.

[8] T.-T. Nguyen, G. Meunier, J.-M. Guichon, O. Chadebec, and T.-S. Nguyen, "An Integral Formulation for the Computation of 3-D Eddy Current Using Facet Elements," *IEEE Trans. Magn.*, vol. 50, no. 2, pp. 549–552, feb 2014.

[9] G. Meunier, O. Chadebec, J.-M. Guichon, V. Le-Van, J. Siau, B. Bannwarth, and F. Sirois, "A-T Volume Integral Formulations for Solving Electromagnetic Problems in the Frequency," *IEEE Trans. Magn.*, vol. 52, no. 3, pp. 1–4, mar 2016.

[10] R. Torchio, F. Moro, G. Meunier, J.-M. M. Guichon, and O. Chadebec, "An Extension of Unstructured-PEEC Method to Magnetic Media," *IEEE Trans. Magn.*, vol. 55, no. 6, pp. 1–4, jun 2019.

[11] G. Meunier, J. M. Guichon, O. Chadebec, B. Bannwarth, L. Krahenbuhl, and C. Guerin, "Unstructured-PEEC method for thin electromagnetic media," *IEEE Trans. Magn.*, vol. 56, no. 1, 2020.

[12] G. Meunier, Q. A. Phan, O. Chadebec, J. M. Guichon, and B. Bannwarth, "Unstructured - PEEC Method with the use of Surface Impedance Condition," *2019 19th Int. Symp. Electromagn. Fields Mechatronics, Electr. Electron. Eng. ISEF 2019*, 2019.

[13] T.-S. Nguyen, T. L. Duc, T.-S. Tran, J.-M. Guichon, O. Chadebec, and G. Meunier, "Adaptive Multipoint Model Order Reduction Scheme for Large-Scale Inductive PEEC Circuits," *IEEE Trans. Electromagn. Compat.*, vol. 59, no. 4, pp. 1143–1151, aug 2017.

[14] M. Fabbri, "Magnetic flux density and vector potential of linear polyhedral sources," *COMPEL - Int. J. Comput. Math. Electr. Electron. Eng.*, vol. 28, no. 6, pp. 1688–1700, nov 2009.

[15] Altair, "Altair Flux™." [Online]. Available: https://www.altair.com/flux/